Chapter 4 : Evolution under irradiation

This chapter is dedicated to the presentation of the results obtained in Louvain-la-Neuve.

The first section deals with irradiations with the quasi-monoenergetic neutron beam in the Q-beam line. This test was aimed to validate the NIEL scaling for neutron energies above 20 MeV.

The second section then presents a summary of the results obtained on CMS test structures: the impact of bias during irradiation is discussed before going into more details about the evolution of the different electrical properties of the sensors.

In this chapter, it is difficult to make assumptions on the shape of the result distributions (is it gaussian or is there another law behind the processes). Every number quoted as standard deviations are to be understood as RMS values of the sample distribution. When required, the propagation of these numbers has been done using the usual variance error propagation formula. The impact of systematic errors is believed to be small compared to these RMS values, according to the results of the inter-calibrations depicted in Chapter 3.

4.1. Experimental neutron hardness factors

As pointed out in 2.3.2, the NIEL hypothesis and the hardness factors, used to scale the fluences of many different particles to a global 1-MeV neutron equivalent fluence, has proven to be useful to describe the depletion voltage and leakage current evolution of silicon devices in a radiative environment. However, these factors have only little experimental confirmation. Regarding neutrons, for instance, there are only 3 experimental measurements at energies below 20 MeV [52].

As the CMS environment will involve neutron energies exceeding 20 MeV, and because the intense fast neutron beam line in Louvain-la-Neuve reaches neutron energies above 20 MeV, it makes sense at this point to perform an experimental determination of the hardness factors above 20 MeV.

For this purpose, a monoenergetic source is obviously always better since the unfolding of the data is easier. By chance, the cyclotron facility in Louvain-la-Neuve has such a neutron beam (refer e.g. to [53]).

This paragraph depicts the experimental determination of NIEL hardness factors at 3 energies above 20 MeV, beginning with a description of the irradiated devices and the beam line.

4.1.1. Diodes description, pre-irradiation qualification

We irradiated several diodes, either oxygenated or not. These were samples received either from CERN (M. Moll) or from the university of Hamburg (G. Lindström).

The devices are all 5X5 mm^2 square pad diodes made on approx. either 280 µm or 300 µm thick silicon wafers (pictured in Fig. 53). Their design is very similar excepted that the Hamburg ones have several guard ring structures, instead of one only for the CERN devices, ensuring a stable high voltage operation and a nice shape of the electric field within the bulk.

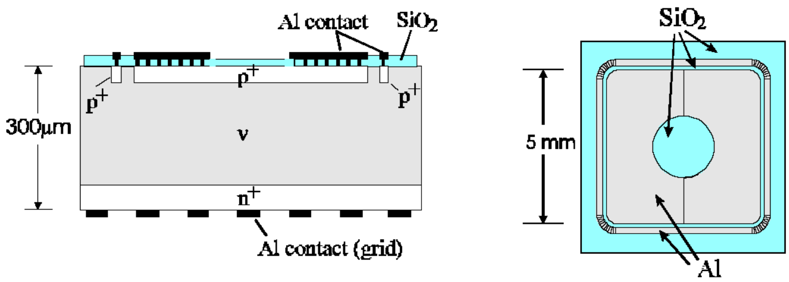

Fig. 53 : Typical silicon pad-diode design, as irradiated in this test (taken from [51]).

The following figures show pre-irradiation CV-IV characterization of those diodes. The results are in agreement with those we received from Hamburg, quoting depletion voltages around 65 V and leakage currents of 0.4 nA for oxygenated silicon or 0.8-0.94 nA for standard silicon.

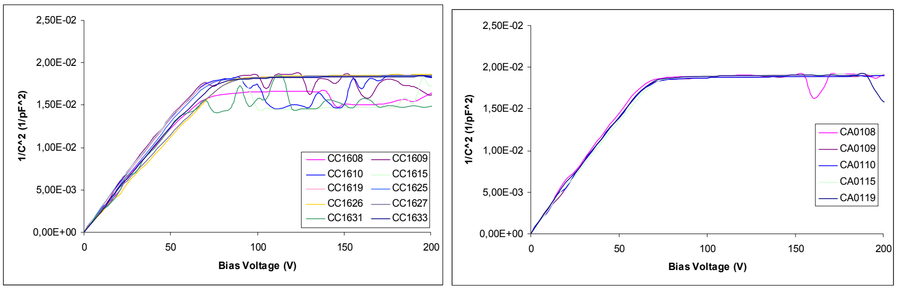

Fig. 54a, b : Oxygenated (left) and standard (right) silicon diodes CV curves before irradiation.

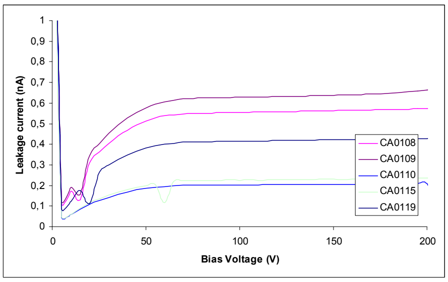

Fig. 55: Oxygenated & standard silicon diodes IV curves before irradiation.

Previous data and literature mention that all these diodes are known to show an “alpha parameter” of 4 10^{-17} A.cm, obtained after proper normalizations of the leakage current shown after irradiation to the volume of the device and to a 1-MeV neutron equivalent fluence (cf. 4.1.3).

4.1.2. Monoenergetic neutron beam line (“Q” beam line)

The details of the quasi-monoenergetic neutron beam are described in [54]. We recall the interesting features for our test, as well as the limitations and drawbacks.

In the so-called Q beam line, neutrons are generated from a primary proton beam hitting an isotopic ^{7}Li target via the ^{7}Li(p,n)^{7}Be reaction (Fig. 56). The remaining charged particles are wiped out of the beam using a magnet and a graphite beam dump.

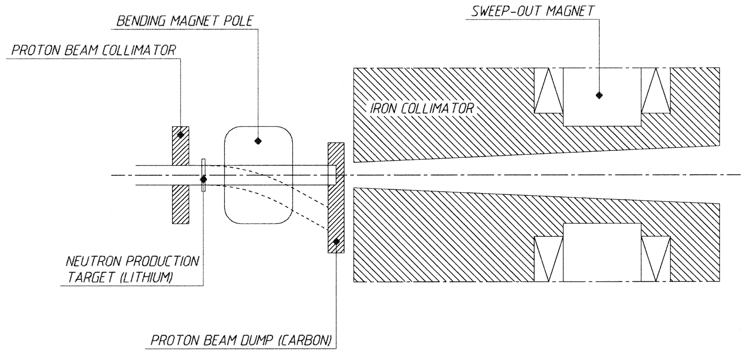

Fig. 56 : Quasi-monoenergetic beam neutron production in Louvain-la-Neuve.

The beam has been characterized for two different target thicknesses [54]. Despite lower neutron fluxes, we preferred the thin (3mm) lithium target to ensure a beam as monoenergetic as possible. The corresponding neutron energy spectra for 3 different proton energies used here are shown in Fig. 57.

We spent 3 days to carry this test, one day for each proton energy. This gives the opportunity to determine NIEL factors well above 20 MeV, where simulations predict a smooth and monotonic behaviour of the hardness factor curve.

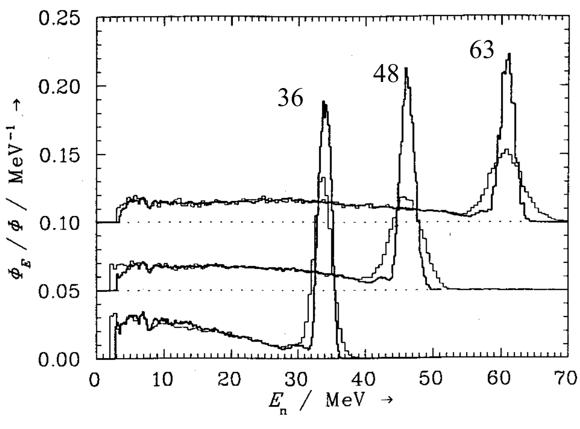

Fig. 57 : Monoenergetic simulated and measured neutron spectra for incident proton energies of 36, 48 and 63 MeV.

Typical fluxes obtained with this facility are around 10^6 n/s with an homogeneity of 10 % within a 30 mm beam spot diameter (at 3 m from the Lithium target). Compared to the intense fast neutron beam line, this flux is smaller by several orders of magnitude.

The fluences reached in the monoenergetic neutron test are therefore very low and causing much less radiation damage. To determine these fluences, we only monitored the intensity of the primary proton beam. We had no other dosimetry system ready for this test since our alanine dosimeters are not sensitive enough and as TLD's would have needed a calibration which we had no time to perform. We obtained integrated proton beam intensities of 228.3 µAh, 237.6 µAh and 187.2 µAh for respective neutron peak energies of respectively 33, 46 and 60 MeV.

The total fluence calculations gave the following values: 6.8 10^{10} n/cm^2, 7.1 10^{10} n/cm^2 and 7.9 10^{10} n/cm^2 for the neutron peak energies of respectively 33, 46 and 60 MeV. Integrated beam measurements and fluence calculations are summarized in Table 12.

Neutron peak energy (MeV)	Integrated proton beam current (µAh)	Fluence at sample position (n/cm^2)
33 ± 2.38	228.3	6.8 10^{10}
46 ± 2.5	237.6	7.1 10^{10}
60 ± 2.61	187.2	7.9 10^{10}

Table 12 : Integrated beam time and fluence summary for the monoenergetic neutron beam.

As a consequence of the low fluences reached, the damage measurements on the diodes have to rely only on the evolution of the leakage current, the depletion voltages being barely affected.

4.1.3. Principle of the test

The radiation-induced variation of the leakage current, discussed in 2.3.3, scales with the normalized fluence and volume of the device. Given the leakage current normalized to the actual neutron fluence, we obtain the total hardness factor of the beam by dividing it by the known alpha parameter found in the literature (e.g. in [32]), which is 3.99 ± 0.33 10^{-17} A/cm (4.3).

$$\Delta I_{leak} = \alpha_{lit.} \Phi_{1-MeV} V \qquad (4.1)$$

$$\Phi_{1-MeV} = \kappa_{beam} \Phi_{real} \qquad (4.2)$$

$$\kappa_{beam} = \frac{\Delta I_{leak}}{\alpha_{lit.} \Phi_{real} V} \qquad (4.3)$$

As mentioned above in this section, we use here the fact that the neutron beam is quasi-monoenergetic. The energy spectrum can be split in 2 parts, and this will help us to compute hardness factors for neutrons above 20 MeV in a way depicted in equations (4.4) trough (4.7).

In the NIEL approximation, the 1-MeV neutron-equivalent hardness factor of a beam is usually computed by folding the energy spectrum with a damage function $\kappa(E)$, which is the total displacement damage normalized to the damage of 1-MeV neutrons (cf. 2.3.2).

$$\kappa_{beam} = \frac{\int_E \frac{d\Phi(E)}{dE} \kappa(E) dE}{\int_E \frac{d\Phi(E)}{dE} dE} = \frac{\int_E \frac{d\Phi(E)}{dE} \kappa(E) dE}{\Phi_{tot}} \qquad (4.4)$$

As we want to obtain the hardness factor of the peak neutrons, we should compute the following hardness factor:

$$\kappa_{peak} = \frac{\int_{E_{treshold}}^{E_{end}} \frac{d\Phi(E)}{dE} \kappa(E) dE}{\int_{E_{treshold}}^{E_{end}} \frac{d\Phi(E)}{dE} dE} = \frac{\int_{E_{treshold}}^{E_{end}} \frac{d\Phi(E)}{dE} \kappa(E) dE}{\Phi_{peak}} \qquad (4.5)$$

$E_{treshold}$ and E_{end} being the two energy limits of the peak region.

As the energy spectrum of the neutron beam is known (Fig. 57), this can be done assuming the hardness factors for energies below the peak are valid.

Naming ‘background” the lower-energy part of the spectrum, we compute the “background” hardness factor using (4.6).

$$\kappa_{bkg} = \frac{\int_0^{E_{treshold}} \frac{d\Phi(E)}{dE}\kappa(E)dE}{\int_0^{E_{treshold}} \frac{d\Phi(E)}{dE}dE} = \frac{\int_0^{E_{treshold}} \frac{d\Phi(E)}{dE}\kappa(E)dE}{\Phi_{bkg}} \tag{4.6}$$

From these 3 last equations we obtain the expression for κ_{peak} in (4.7).

$$\kappa_{beam} = \frac{\int_0^{E_{treshold}} \frac{d\Phi(E)}{dE}\kappa(E)dE + \int_{E_{treshold}}^{E_{end}} \frac{d\Phi(E)}{dE}\kappa(E)dE}{\Phi_{tot}}$$

$$\frac{\int_{E_{treshold}}^{E_{end}} \frac{d\Phi(E)}{dE}\kappa(E)dE}{\Phi_{tot}} = \kappa_{beam} - \frac{\int_0^{E_{treshold}} \frac{d\Phi(E)}{dE}\kappa(E)dE}{\Phi_{tot}}$$

$$\frac{\int_{E_{treshold}}^{E_{end}} \frac{d\Phi(E)}{dE}\kappa(E)dE}{\Phi_{tot}} \frac{\Phi_{tot}}{\Phi_{peak}} = \left(\kappa_{beam} - \frac{\int_0^{E_{treshold}} \frac{d\Phi(E)}{dE}\kappa(E)dE}{\Phi_{tot}} \frac{\Phi_{bkg}}{\Phi_{bkg}} \right) \frac{\Phi_{tot}}{\Phi_{peak}}$$

$$\kappa_{peak} = \left(\kappa_{beam} - \kappa_{bkg} \frac{\Phi_{bkg}}{\Phi_{tot}} \right) \frac{\Phi_{tot}}{\Phi_{peak}} \tag{4.7}$$

The analysis at the three different neutron peak energies is done assuming the published hardness factors are valid over the whole energy range and this, independently of the results obtained for lower energies during the higher energy irradiations.

Starting the interpretation of data with the 33 MeV data and going further on with increasing energy up to 46 and 60 MeV, the results will either confirm the values in the literature or, in case of discrepancies, will give an idea of the point where the experimental NIEL hardness factors start to diverge from the simulated ones.

4.1.4. Post-irradiation measurements and calculations

Before going through the analysis of the leakage current, a few CV measurements performed on the irradiated diodes are useful to illustrate the above mentioned fact that depletion voltages are barely affected by the irradiations. This is pictured in Fig. 58, where one clearly sees that the kink locating the depletion voltage is located at very similar positions, not only at the different annealing stages after irradiation, but also before and after irradiation. The differences in the evaluated depletion voltages between all measurements is less than 5 V.

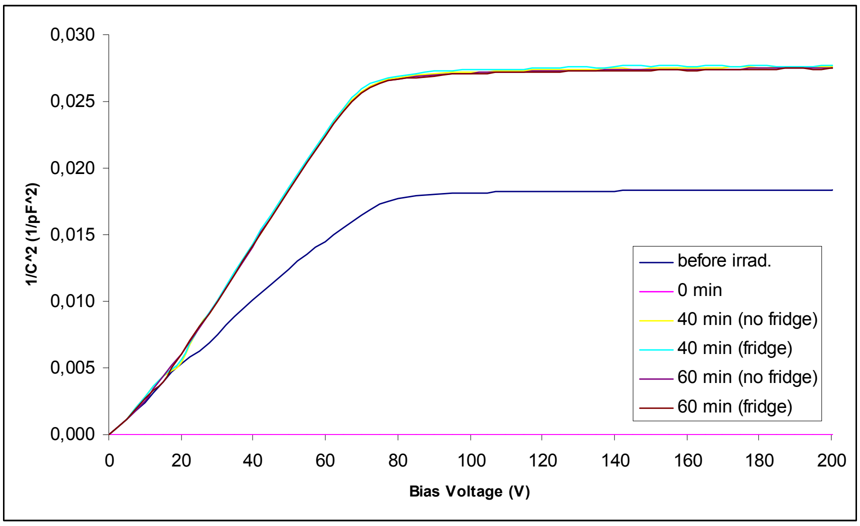

Fig. 58 : Comparison of the CV curves before and after irradiation for each annealing step on diode cc16-09, irradiated with 33 MeV neutrons at a fluence of 6.8 10^{10} n/cm^2.

The IV measurements were performed with the guard ring of the diodes connected in order to keep control of the volume concerned with the leakage current. This leads to a better estimation of the alpha parameter used to determine the hardness factor of the beam and hence to obtain more reliable hardness factors. Another key point when performing measurements after heat treatments is the impact of a radiation-induced and heat-activated bistable defect [43], which can artificially increase the leakage current right after the annealing treatment. The comparison of the curves labelled “fridge or “no fridge” for a given annealing time on Fig. 59 illustrates the fact that this bistable defect has no or only small impact in the case of the irradiations performed here. Indeed, difference of leakage current between measurements performed right after the heat treatment and then after some time in a fridge is of the order of two percent (0.5 nA over about 35). This is probably due to the low fluence reached and the relatively short annealing steps between measurements. However, care has been taken to leave the structures in a fridge for one night between each annealing step and the measurement. Measurements were done around 20 °C and corrected for the small temperature offset of the chuck.

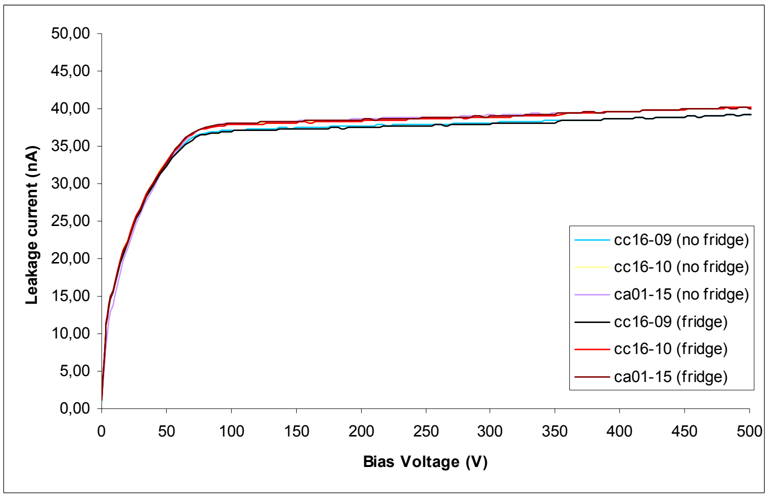

Fig. 59 : Comparison of the leakage current on diodes pre- and post-storage in a fridge after an annealing step of 20 minutes at 60 °C. The diodes were irradiated with 33 MeV neutrons for a real fluence of 6.8 10^{10} n/cm^2.

The tests were also performed after different annealing steps to check whether the annealing curves match those published in the literature. On Fig. 60 (where the data are already normalized using the total beam hardness factors computed below), the alpha parameter annealing points are shown for all diodes measured in this test. These are found to be close to published curves and thus the following sections will only report on the leakage current values after 80 minutes at 60 °C, the most widely used annealing condition for silicon devices*, for which the alpha parameter has widely been studied.

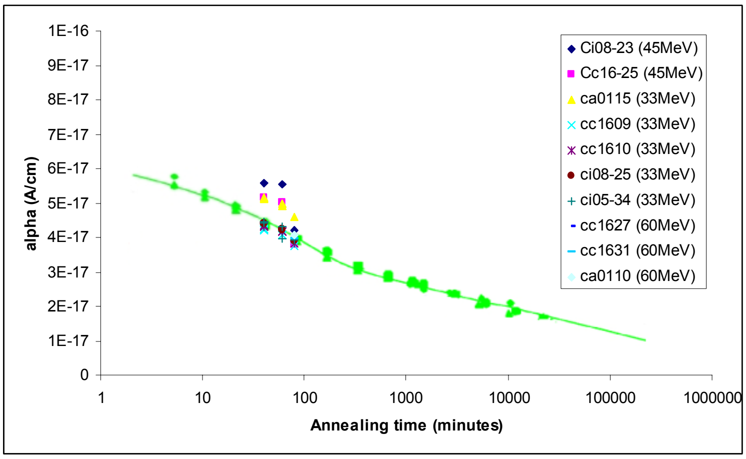

Fig. 60 : Evolution of the alpha parameter measured on the diodes for different neutron energies, compared to literature [32].

4.1.4.a. Measurements at 33 MeV

The variation of the average leakage current obtained with 5 diodes (whether oxygenated or not, these show the same leakage current) is 51.7 ±13 nA. Using equations (4.1) to (4.3), this corresponds to a 1-MeV equivalent fluence of $1.29\ 10^{11} \pm 4.85\ 10^{10}$ n/cm^2.

The actual neutron fluence, obtained from the integrated proton beam current and the neutron beam calibration, is $6.8\ 10^{10}$ n/cm^2 (cf. Table 12) and hence the global hardness factor for the 33 MeV neutron beam is 1.90 ± 0.16. Applying equation (4.7) with a computed background hardness of 1.77, one obtains a 33 MeV hardness factor of 2.05 ± 0.56.

4.1.4.b. Measurements at 46 MeV

The same method has been applied to the readings of the leakage current obtained with diodes irradiated with 46 MeV neutrons. The average increase of the leakage current observed is of 43.6 ± 3.4 nA corresponding to a 1-

* Corresponding to approximately 14 days at room temperature, it offers a good control of the annealing and is less sensitive to oven temperature variations than it's 4 minutes at 80 °C alternative.

MeV neutron equivalent fluence of 1.56 10^{11} ± 1.12 10^{10} n.cm^2 whereas the total actual fluence is 7.07 10^{10} n/cm^2.

The beam hardness parameter obtained is hence 2.20 ± 0.17, for a background hardness factor found of 1.90. The computed hardness factor for peak neutrons at 46 MeV is 2.58 ± 0.66, not exactly matching 1.9 as quoted in [42], but this value is almost within our errors.

4.1.4.c. Measurements at 60 MeV

The increase of the average leakage current is 38.1 ± 0.6 nA. Divided by the diode volume and the usual 3.99 10^{-17} A/cm alpha parameter, a 1-Mev equivalent fluence of 1.36 10^{11} ± 2 10^{9} n/cm^2 is obtained. Dividing again this result with the tabulated actual fluence of 7.87 10^{11} n/cm^2, the corresponding beam hardness factor is 1.72 ± 0.02.

In spite of the results obtained at 46 MeV, the tabulated hardness factors found in [42] have been used to compute a background hardness factor of 1.98 in the case of the 60 MeV neutron beam.

These considerations lead to a 60 MeV neutron experimental hardness factor of 1.26 ± 0.61, much lower than the 46 MeV one, but compatible with the value quoted in the literature (1.64).

4.1.5. Summary and comparison with literature

As foreseen from the neutron fluxes and fluences reached, a few measurements on the irradiated diodes proved that the depletion voltage of the diodes were barely affected by the irradiation; we are thus left with the single possibility to determine hardness factors using the increase of the leakage current. This increase, if considerably lower in this test than with the CMS tests concerned in the next sections, has been found to be large enough to be accurately measured with the probe station and its associated equipment, taking care to keep it light tight to avoid any perturbation of the measurement.

The results are summarized in Table 13 and compared to previous data in Fig. 61.

Neutron peak energy (MeV)	Hardness factor
33 ± 2.38	2.05 ± 0.56
46 ± 2.5	2.58 ± 0.66
60 ± 2.61	1.26 ± 0.61

Table 13 : Summary of the experimental hardness factor determination results.

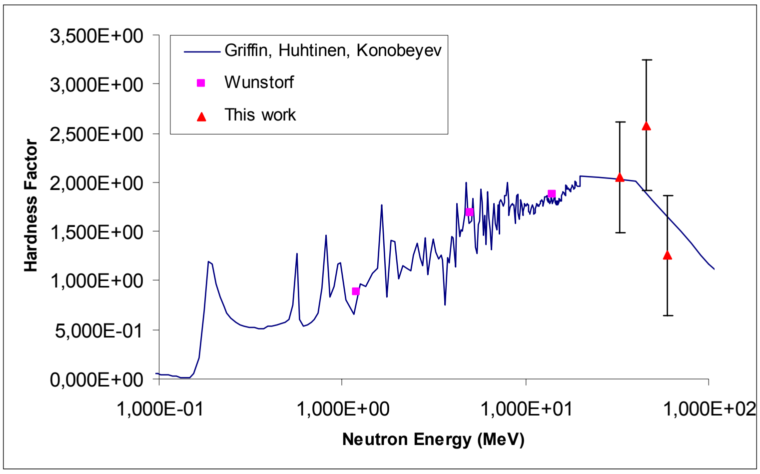

Fig. 61 : Neutron hardness factors as compiled from literature ([42] and [52]) compared to results obtained at Louvain-la-Neuve with the monoenergetic neutron beam line.

Our data point at 33 MeV neutron peak energy matches with 2.04, quoted for neutrons of 30 MeV in [41] or [42]. The results obtained at 46 and 60 MeV are not on the curve quoted in the literature. However, the error bars do not allow to draw any conclusion pointing towards the fact that previous simulations are wrong. Furthermore, the fact that the results are either higher or lower than the latter do not even indicate any tendency of the hardness factors to be actually lower than those quoted here, as expected by some [55].

4.2. Analysis of CMS test structures

This section is dedicated to the results obtained during the irradiation of the CMS tracker sensors. During the years 2001 to 2004, we performed in this context the irradiation of more than 460 test structures and 25 full-sized sensors, sampling the major part of the production from both vendors (ST microelectronics and Hamamatsu photonics). This gave us a unique opportunity to study the evolution of all relevant electrical properties on a statistical basis.

In this scope, we obtained some fluence-related evolutions of the parameters and investigated on the influence of bias during irradiation. Before entering into the details of the statistical analysis, two sections will be dedicated to MOS devices and interstrip capacitances which have a completely different behaviour before and after irradiation. Other parameters, linked to the bulk or surface-related damage are investigated afterwards.

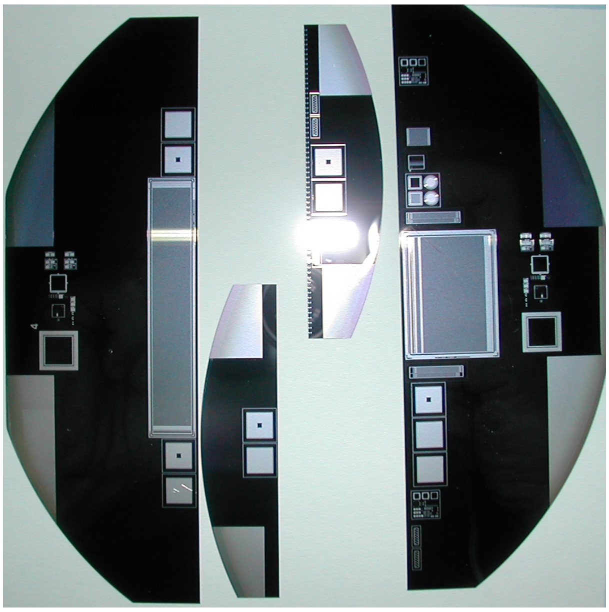

Fig. 62 : The 4 half moons cut around a Hamamatsu sensor (the standard structure is the right one).

Let us introduce here the CMS test-structures. They are produced with the cut-off pieces left around the full-sized sensors after dicing of the silicon wafer. Their production does not lead to major additional costs and it offers a great opportunity to make specific structures useful to check the quality of the sensors and to perform a wide range of tests without damaging the useful active part of the wafer. Due to their rounded shape, they are called “halfmoons” (Fig. 62). Among the four halfmoons produced on every wafer, one of these remains the same for all detector designs.

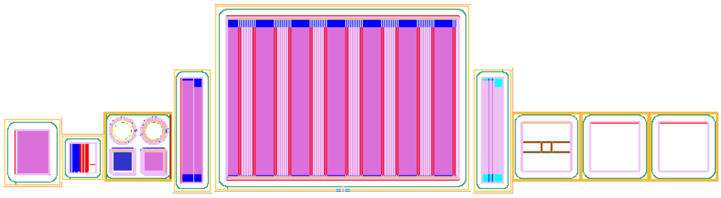

Fig. 63 : The standard CMS test-structure devices.

Pictured on Fig. 63, this test structure has (from left to right):

- An array of 26 AC-coupled strips like those present on the sensors, without the bias resistors;
- A set of nine structures dedicated to the measurement of resistances: three implant strips, three bias resistors, three aluminium strips;
- A set of four gate controlled diodes among which two square and two round ones;
- A second array of AC-coupled strips, but now the aluminization of these are connected together to facilitate grounding;
- A small-sized silicon strip detector (baby detector) with all features of the full-sized one;
- A third array of AC-coupled strips, but this time these strips are not connected in any way to a bias ring;
- A photodiode, quite similar to planar test diodes used e.g. by the RD48 collaboration when elaborating the HH model;
- Two MOS devices.

This set of nine test structures allow an accurate characterisation of all parameters of the silicon sensor and the small-sized strip detector serves as a reference structure for our irradiation tests.

The baby detector has 192 strips, placed 120 µm apart from each other. As a replica of the full-sized model, it has 1.5 MΩ bias resistors, a bias ring and a guard ring. Until the end of this chapter, all measurements are performed on this device unless otherwise stated.

4.2.1. The impact of bulk biasing during irradiation

The first study presented here will be the impact of the bias voltage during irradiation on the electrical properties of the so-called "baby detectors", built on the CMS standard test structures. As mentioned in 2.3.5, previous studies have been published in the literature, and we would like to compare their results in the context of our own work.

The sample studied here is made of 60 structures of both thicknesses, irradiated during the last tests of 2004. These have been chosen because they were made by a single vendor (Hamamatsu) and they have all been submitted to the same manufacturing process (not modified during their production). All of them passed the whole CMS irradiation qualification process and all have very similar initial properties (e.g. resistivity). The irradiation has been performed as usual with neutrons, at a temperature of – 10 °C and under 600 V bias for the biased structures. The post-irradiation annealing is also standard (80 minutes at 60 °C) and the structures have been left afterwards for at least one night in the fridge before any measurement. The reference bias voltage for all strip parameters is 400 V, as defined in the CMS-IQC protocol.

This section deals only with the impact of bias on the evolution of the electrical properties. Hence we do not go into much detail: it is not necessary to perform a study in terms of e.g. the Hamburg model. However, as fluences vary from structure to structure, it is relevant to look at some variables using a normalization based on fluences. We will see here that the tests did not show any impact of the bias in our case.

Bulk parameters

Before entering into the details of measurements on the strips, let us take a look at the bulk properties, focusing on the macroscopic measurements of leakage current and depletion voltage.

Fig. 64 plots the fluence as a function of the total leakage current for baby detectors after irradiation. For every graph in this section, diamonds show the results of irradiation-biased structures and squares show the results of unbiased ones.

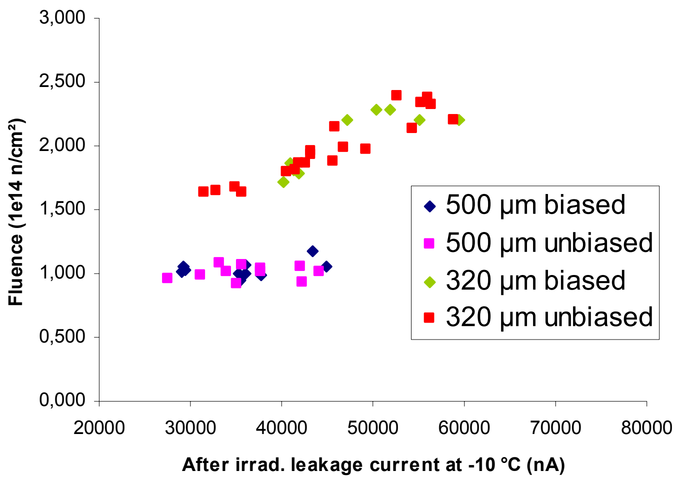

Fig. 64: Post-irradiation leakage current of biased and unbiased standard test structures.

As in Fig. 64, the leakage currents for thick and thin structures do not allow to decide upon any influence of the bias during irradiation. For similar fluences, the biased and unbiased samples of the same thickness give similar leakage currents. When we compare the average values of the alpha parameter measured at –10 °C, we obtain the following:

Structures	Average value (nA/cm)
320 µm - Biased	2.19 ± 0.39
320 µm - Unbiased	2.18 ± 0.18
500 µm - Biased	2.62 ± 0.55
500 µm - Unbiased	2.18 ± 0.25

Table 14 : Biased-unbiased alpha parameter comparison.

This clearly shows that the bias voltage does not seem to have any impact on the bulk leakage, hence confirming the observations made by Cindro et al [35], where permanently biased or unbiased structures have shown to have the same leakage currents. It also gives a first confirmation of the well-known result that the alpha parameter does not depend on the initial bulk resistivity of the material. We will give more details about this later.

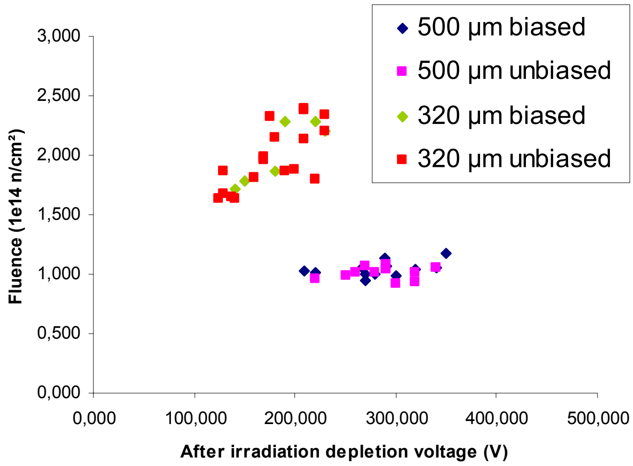

Fig. 65 : Post-irradiation depletion voltages of the biased-unbiased sample.

Fig. 65 gives the same plot for the depletion voltages after irradiation. On each sample, the average values and standard deviations of depletion voltages and fluences are in fact compatible for structures of the same type :

	Biased	Unbiased
Thick structures	$<\Phi_{1\ MeV}>=1.03\pm0.06\ 10^{14}n/cm^2$	$<\Phi_{1\ MeV}>=1.02\pm0.07\ 10^{14}n/cm^2$
	$<V_{dep}>=283\pm42$ V	$<V_{dep}>=294\pm45$ V
Thin structures	$<\Phi_{1\ MeV}>=2.05\pm0.22\ 10^{14}n/cm^2$	$<\Phi_{1\ MeV}>=2.98\pm0.25\ 10^{14}n/cm^2$
	$<V_{dep}>=185\pm36$ V	$<V_{dep}>=178\pm35$ V

Table 15 : Average and standard deviation values of the depletion voltages.

To confirm all this in a quantitative way, we performed and compared linear regressions on the data from each sample.

This approximation of the Hamburg model is valid since all the fluences concerned here are well above those for type inversion: the effective doping concentrations for a given fluence and for a single annealing step at a given temperature, can then be considered as a linear function of the 1-MeV equivalent fluence (4.8). Indeed, for high resistivity silicon, the constant c is usually above 20 10^{-14} cm^2/n. Moreover, at a fluence of 10^{14} n/cm^2 the non-linear term is well below 10^{-9}.

$$N_{eff}(\Phi_{eq}, t_a, T_a) = N_{eff,0}\left(1 - r(1 - e^{-c\Phi_{eq}})\right) - \Phi_{eq}\left(g_c + g_a e^{-\frac{t_a}{\tau_{a,T_a}}} + g_y(1 - e^{-\frac{t_a}{\tau_{y,T_a}}})\right) \quad (4.8)$$

Unfortunately, our samples are composed of structures irradiated at very similar fluences, and the uncertainties on fluences and depletion voltages lead to large errors on the regression coefficients, and consequently to high χ^2 for every regression. The results were that the obtained regression parameters were compatible with each other (no influence of biasing during irradiation), but also that the statistical significance was very low. Therefore we confirm our initial statement: according to our experience, bias has no influence on the depletion voltage.

This result seems somewhat different from the one quoted by Cindro et al ([35] and [36]), where permanently biased structures have shown different effective doping concentration compared to unbiased ones. When permanently biased, those structures have effective doping concentration twice as high as those for the unbiased structures. This has been discussed above, and there is no discrepancy with our results as the difference of the depletion voltage tends to vanish if both samples are left unbiased for a period about 50-100 h: this was the case in our conditions.

A further compatibility check would be to bias our detectors for a much longer period and see if the full depletion voltages rise. This test would need new irradiations and a careful annealing in conditions similar to those pictured in [35], as any annealing behaviour is highly temperature-dependent.

Strip parameters

We did not find any impact of bias during irradiation on the bulk parameters. But is it the same for strip properties like bias resistors, the coupling and interstrip capacitances? This is what we quickly inspect in the present paragraph. Let us start with the bias resistors.

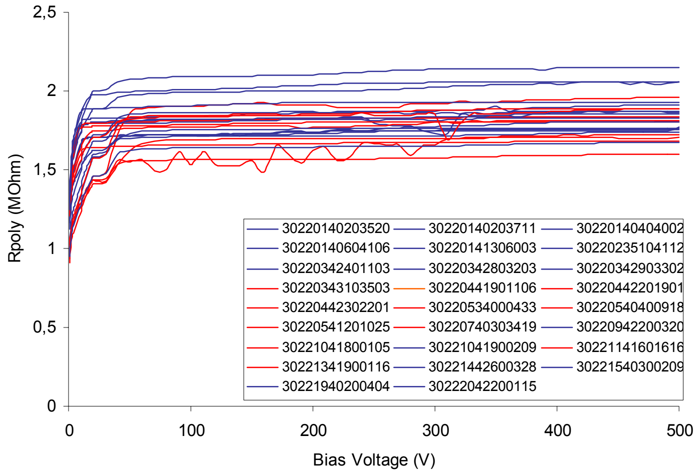

Fig. 66 : After irrad. R_{poly} ramps on biased (red) and unbiased (blue) thick and thin structures.

As shown above, the measurements of the bias resistor quickly reach saturation values, even on a slightly biased detector. Also, according to the distributions of the variations (Fig. 67), it seems that the impact of irradiations is very limited and seems to be fairly independent of the dose.

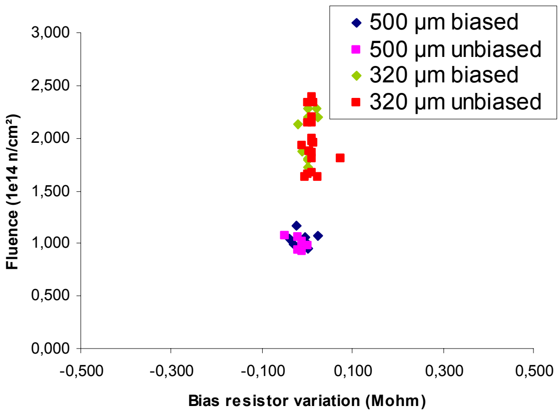

Fig. 67 : Variation of the bias resistors on biased/unbiased samples, taken at 400 V bias.

Due to this apparent independence on the dose, we will directly look at the variations of the average values of the resistors: indeed the relative variations are found to be less than a percent. The average values and standard deviations of the samples are listed in Table 16. As for the bulk parameters, they again point towards damages independent of bias.

	Biased	Unbiased
Thick structures	<ΔR_{poly}>=-1.07±1.73 %	<ΔR_{poly} >=-0.92±0.86 %
Thin structures	<ΔR_{poly} >=0.14±0.74 %	<ΔR_{poly} >=0.60±0.94 %

Table 16 : Average & standard deviation values for the bias resistor variation of biased and unbiased samples.

The coupling capacitances, like polysilicon resistors, quickly reach a saturation value when the device starts to be biased. Hence, a simple look at the distributions of variations will give a first clue of the possible dependence on bias.

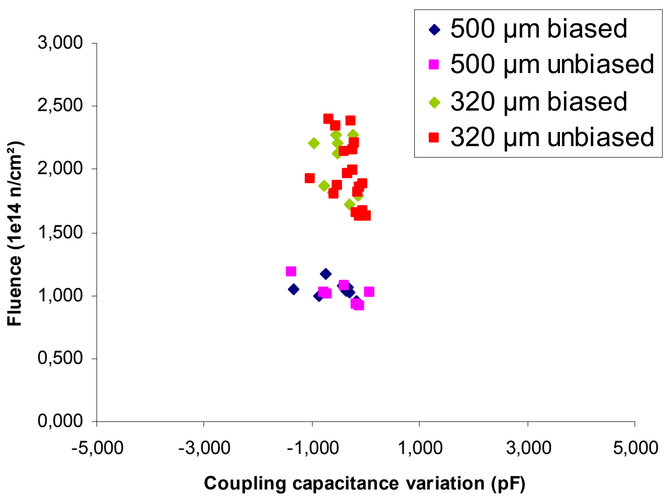

Fig. 68 : Coupling capacitance variation distributions on biased/unbiased samples, taken at 400 V bias.

Once again, from Fig. 68 there is no clear fluence dependence of the damage of the coupling capacitance. It is therefore interesting to look at averages and standard deviations of the samples (Table 17). Given these averages, one deduces a slight decrease of the coupling capacitances with irradiation, but no bias effect.

	Biased	Unbiased
Thick structures	$<\Delta C_{AC}>=-0.84\pm0.57$ %	$<\Delta C_{AC}>=-0.72\pm0.73$ %
Thin structures	$<\Delta C_{AC}>=0.75\pm0.39$ %	$<\Delta C_{AC}>=0.45\pm0.38$ %

Table 17 : Average & standard deviation values for the coupling capacitance variation of biased and unbiased samples.

About the interstrip capacitances, we have to consider their evolution with the sensor bias. Indeed, the interstrip capacitances do not reach a saturation value early in the bias ramp but instead show a decrease well above the depletion voltage. However, the large plateau in these curves allows us to use the standard test results anyway*, considering a bias level around 0.8 V_{dep}. In this way, we obtain the now usual distributions over fluence (Fig. 69).

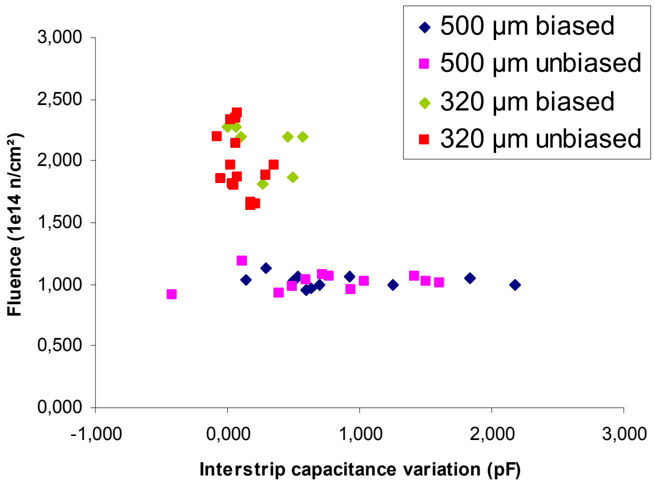

Fig. 69 : Distributions of the variations of the interstrip capacitance for biased/unbiased samples, taken at 400 V bias.

* Standard results are taken as the parameter value at 400 V bias.

One directly notices that all samples show an increase of the interstrip capacitance, but also that thick structures show a much broader spread of the variation of the capacitances. Both the increase and spread are directly related to the C_{int} saturation, and will hence not be discussed here, but later in this chapter. However and once again, the distributions seem to be similar for both biased and unbiased devices. The averages and standard deviations of each sample tend to confirm this statement, and we therefore conclude there is no evidence of a bias effect on the interstrip capacitances.

	Biased	Unbiased
Thick structures	$<\Delta C_{int}>=0.84\pm0.57$ pF	$<\Delta C_{int}>=0.69\pm0.63$ pF
Thin structures	$<\Delta C_{int}>=0.28\pm0.23$ pF	$<\Delta C_{int}>=0.10\pm0.12$ pF

Table 18 : Average and standard deviation values for the interstrip capacitance variation of biased and unbiased samples, taken at 400 V bias.

The interstrip resistances have a behaviour much more dependent on the bias conditions. Hence, it is crucial to look at the graphs showing these resistances as a function of the bias voltage than simply looking at the distribution of the scan values for a given bias voltage.

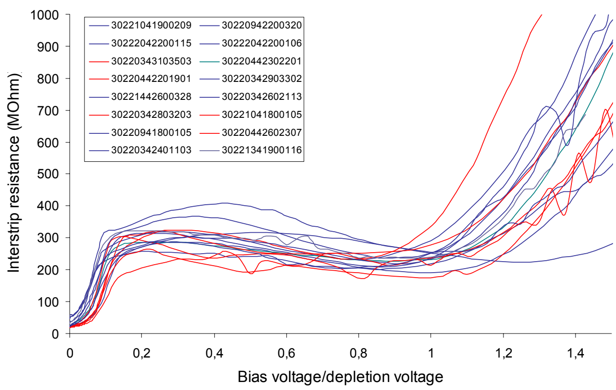

Fig. 70 : Interstrip resistance as a function of normalised bias for thick structures - Red lines show the results for the irradiation-biased structures.

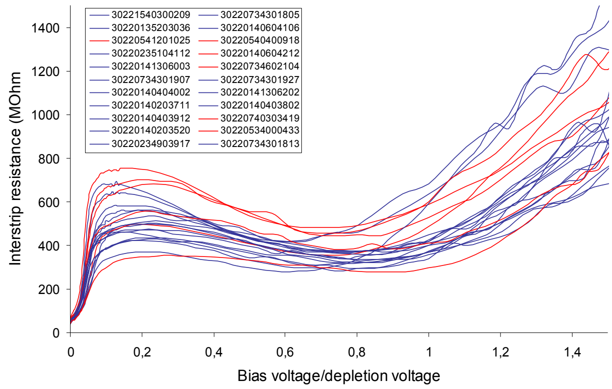

Fig. 71 : Interstrip resistance as a function of normalised bias for thin structures - Red lines show the results for the irradiation-biased structures.

All curves on Fig. 70 and Fig. 71 have seen their ordinates (the bias voltage) individually scaled according to the depletion voltages of the structures. This makes the comparison between all curves easier, and highlights their common features.

It is obvious that all scaled curves show the same behaviour, with a local minimum at about 0.8 V_{dep}. Fig. 72 then shows the Interstrip resistance versus fluence distribution at this bias.

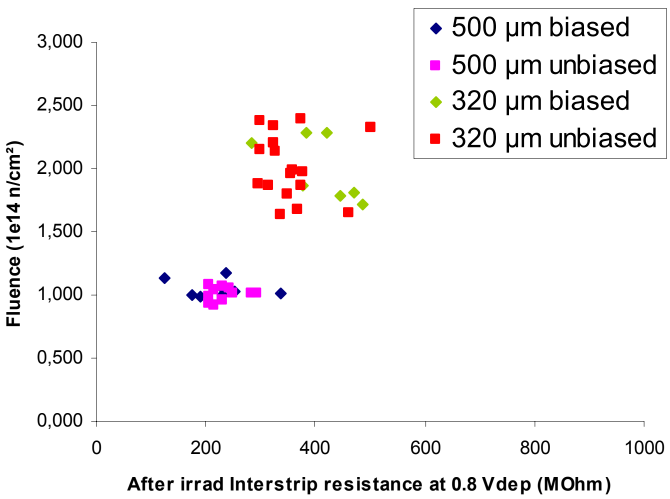

Fig. 72 : Interstrip resistance distributions on biased/unbiased samples.

Like in other cases, we do not see a clear correlation between interstrip resistance values and fluences. Table 19 summarises the average values and standard deviations on the samples: once again no influence of bias can be deduced.

	Biased	Unbiased
Thick structures	$\langle R_{int} \rangle$=222±58 MΩ	$\langle R_{int} \rangle$=224±30 MΩ
Thin structures	$\langle R_{int} \rangle$=409±69 MΩ	$\langle R_{int} \rangle$=354±54 MΩ

Table 19 : Average and standard deviation values for the interstrip resistance for biased and unbiased samples.

4.2.2. Summary of the irradiation results

Although we started the irradiations back in 2001, the data used for this analysis have mainly been collected during the 2003-2004 irradiations. This is due to the setup attached to the probe station which has been finalised after the second IQC workshop, held in Louvain-la-Neuve in May 2003. Hence, only the data collected thereafter are free of any setup-related constraint. The concerned data sample is made of data gathered on 228 structures and sensors, produced by both Hamamatsu and STM. As it has been demonstrated in the previous paragraph that the obtained results are independent of whether the device was biased during irradiation or not, we will consider here both cases within the same sample.

Bulk properties: leakage current

The comparison of the leakage current results with literature imposes a temperature correction of our measurements of the leakage current, obtained at −10 °C, to a standard temperature of 20 °C.

According to equation (2.4), the correction factor before irradiation is of 15.2. An experimental determination of this scaling factor gave 16.2 ± 0.5 for a CMS baby detector; and 18.3 at a reference 400 V bias voltage. But is this still valid after irradiation, or does the higher concentration of defects influence the leakage current so that it varies differently with the detector temperature? In order to check this, a measurement of the leakage current as a function of bias has been carried out for temperatures varying between –10 °C to 23 °C in steps of 1 °C. The results are discussed below.

Te device is a thin Hamamatsu baby detector, irradiated at a fluence of 2.22 10^{14} n/cm² and annealed as usual for 80 minutes at 60 °C. It has been cooled down in a fridge for a night between the annealing treatment and the measurement itself.

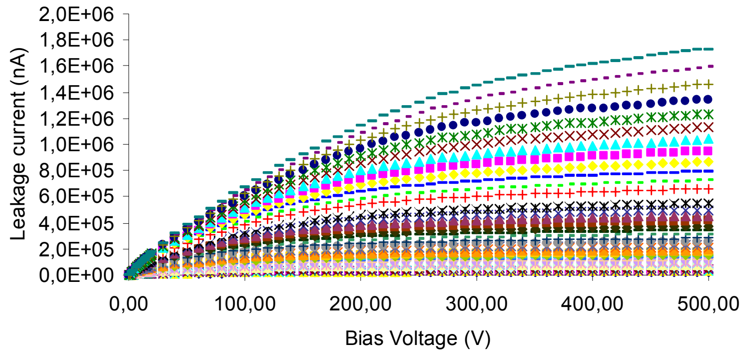

Fig. 73 : The leakage current of a baby detector after irradiation, at different temperatures.

The leakage current scaling factor from –10 °C to 20 °C, averaged over the entire curve, is of 15.6, to be compared with a theoretical factor of 15.54. At our reference bias voltage of 400 V, used by the collaboration to compare all leakage currents, the scaling factor is of 21.71, hence a bit higher than for a non-irradiated structure.

The post-irradiation measurements were performed at –10°C, this has been decided as the tracker will be operated cold, but also because the leakage current of irradiated full-size sensors may become too high for the power supply used in the different CMS probing labs. Hence this scaling factor is useful when considering a comparison with the literature.

Fig. 74 shows the distribution of the alpha parameter observed during our neutron irradiation tests. The observed alpha parameters observed, once scaled to 20 °C, are of 3.77 ± 0.64 10^{-17} A/cm for thin structures and 4.23 ± 0.61 10^{-17} A/cm for thick ones. Considering the whole set of measurements as a simple data set gives an alpha parameter of 4.23 ± 0.8 10^{-17} A/cm, to be compared with 3.99 ± 0.03 10^{-17} A/cm in [32].

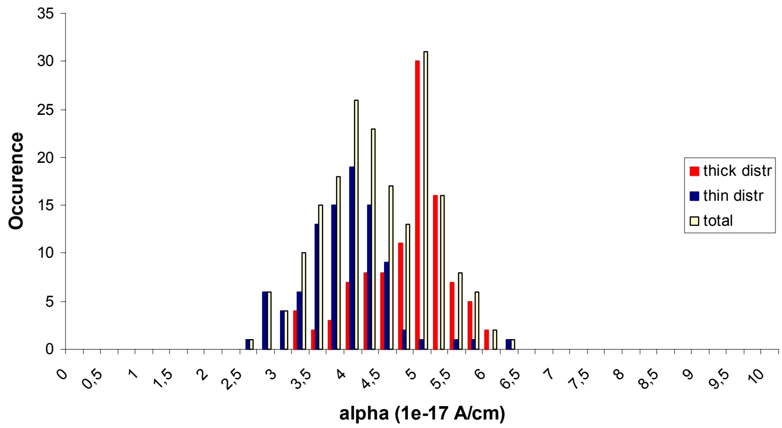

Fig. 74 : alpha distribution for thick and thin structures.

The leakage current obtained during the CMS irradiations is thus compatible with literature. A possible source for the difference in the averages and the spread of the distribution may be found in the fact that our measurements were not performed with a connected guard ring, leading to possible uncertainties on the size of the volume from which the current is drawn. The fluence uncertainty plays also a major role in the distribution spread.

Bulk properties: depletion voltage

At the occasion of the first neutron irradiations, standard RD48 diodes were put in the beam to get another reference for the fluence determination. This has been the occasion to perform an early annealing study at a temperature of 40°C to slow down the annealing processes.

This annealing study has been useful to show that the fluence normalisation is fine, as only the reverse annealing time constant had to be a bit changed from literature data. The results are shown on Fig. 75, where the experimental measurements are compared to predictions of the model. The parameters used here are quoted in Table 20.

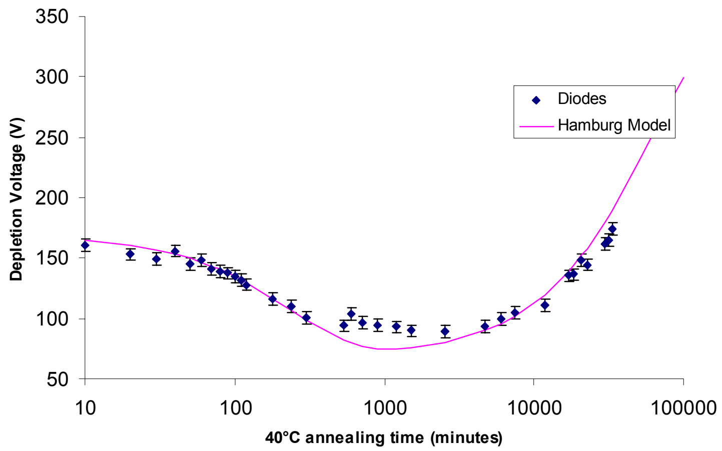

Fig. 75 : Standard diode annealing curve at 40°C.

Stable damage	$G_c = 1.5\ 10^{-2}$ 1/cm	$N_{c0}/N_{eff,0} = 0.8$	$C^*N_{eff,0} = 0.109$
Beneficial annealing	$G_a = 1.81\ 10^{-2}$ 1/cm	$\tau_a = 240$ min	
Reverse annealing	$G_y = 5.16\ 10^{-2}$ 1/cm	$\tau_y = 60000$ min	

Table 20 : Parameters used in the Hamburg model to compare expected values of the depletion voltage with the experimental data of the first irradiated diodes.

Coming to the irradiation of the CMS baby detectors, the application of the Hamburg model becomes a bit more difficult. As a reminder, the Hamburg model predicts in fact the evolution of the effective doping concentration as a function of the 1-MeV equivalent fluence and heat treatment of the detector. To compare the depletion voltages determined with the probe station, the model prediction has to take into account the effects of the geometry of the sensor to the depletion voltage as mentioned on page 35, equation (2.6).

On Fig. 76 and Fig. 77, a summary of all post-irradiation depletion voltages obtained in 2003-2004 is given, together with the Hamburg model predictions for a thick and a thin structure having the same geometry as standard CMS baby detectors, and with the average initial doping concentration observed during the production phase. Also, a thickness of 290 µm instead of 320 µm has been used according to HPK recommendations about the thin structures. This is due to a special wafer treatment we have not much details about.

The parameters injected in the Hamburg model to match these depletion voltages are given in Table 21 for the high resistivity sensors, in Table 22 for the thin low-resistivity ones. These parameters are directly taken from M. Moll's PhD thesis [32]. Using these parameters, an estimation of the depletion voltage using the Hamburg model has been computed for each structure, taking its geometry and initial depletion voltage into account. The average deviation of the predicted depletion voltage to the predicted one is found to be as less as 1 V. Unfortunately, the standard deviation of this deviation is about 70 V due again to the fluence spread.

Stable damage	$g_c = 1.56\ 10^{-2}$ 1/cm	$N_{c0}/N_{eff,0} = 0.56$	$C^*N_{eff,0} = 0.069$
Beneficial annealing	$g_a = 2.01\ 10^{-2}$ 1/cm	$T_a = 24.1$ min	
Reverse annealing	$g_y = 4.92\ 10^{-2}$ 1/cm	$T_y = 1010$ min	

Table 21 : Parameters used in the Hamburg model to fit the depletion voltage data of CMS 500 µm thick test structures.

Stable damage	$g_c = 1.43\ 10^{-2}$ 1/cm	$N_{c0}/N_{eff,0} = 0.64$	$C^*N_{eff,0} = 0.09$
Beneficial annealing	$g_a = 1.67\ 10^{-2}$ 1/cm	$T_a = 15.4$ min	
Reverse annealing	$g_y = 5.16\ 10^{-2}$ 1/cm	$T_y = 1160$ min	

Table 22 : Parameters used in the Hamburg model to fit the depletion voltage data of CMS 320 µm thin test structures.

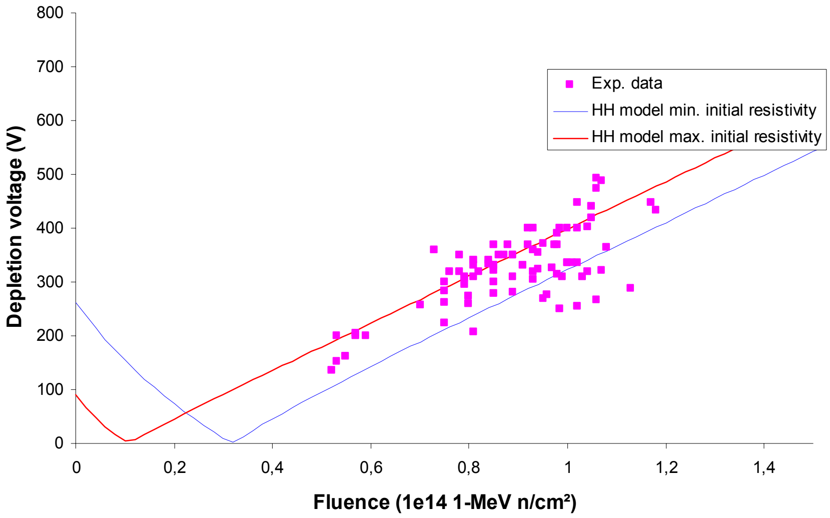

Fig. 76 : Post-irradiation depletion voltages obtained during the neutron irradiation tests in Louvain on 500 µm-thick CMS structures.

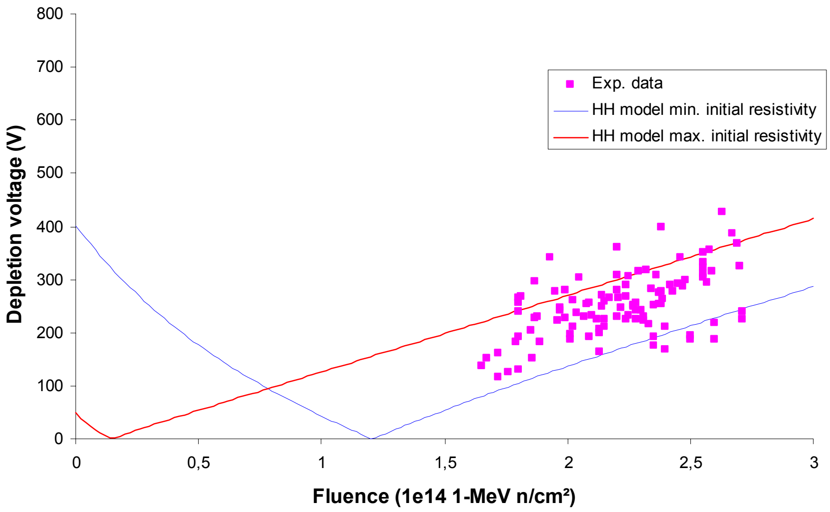

Fig. 77 : Post-irradiation depletion voltages obtained during the neutron irradiation tests in Louvain on 320 µm-thick CMS structures.

It is difficult, considering the depletion voltages obtained here, to obtain a better estimation of the Hamburg model parameters for the CMS structures. Indeed, given the fact that the average deviation to the model is small, an accurate re-estimation of these parameters would require an irradiation campaign at various different fluences, with several devices at each fluence and an annealing study for each of them.

It is also worth mentioning that the value of the reverse annealing parameters plays only a minor role on the interpretation of the results: with a single annealing step of 80 minutes at 60 °C, beneficial annealing is already well in progress whereas reverse annealing is only in its very early stage (with $1\text{-}e^{-80/Ty}$ being equal to 0.062 in equation (2.12), page 45). However, if all the other parameters were well-known, a fit of the annealing time constants with a single annealing state of the sensors would lead to a poor confidence in the fit results. Further discussions on these time constants will be found in S. Assouak's thesis.

Nevertheless, it is amazing to see that the parameters quoted in the literature give such a good idea of the evolution of the depletion voltage under neutron irradiation.

Triggered by a paper written by M. Mikuz et al. [37], a late study of the stability of the depletion voltage after irradiation has been done. This study was aimed to check whether the depletion voltage of an irradiated device raises when the structure is kept biased for a long time. The results quoted in the paper showed that the depletion voltage raises if the object is kept at room temperature, but nothing was indeed quoted for a device kept cold, as will be the case in CMS.

This stability measurement has been performed on a HPK IB1 test structure, irradiated in late 2004 at a fluence of $1.96\ 10^{14}$ n/cm². Like other structures, it has been annealed for 80 minutes at 60 °C. Its depletion voltage has been measured daily during 2 months and the structure has been kept biased at 400 V between measurements.

During the first phase of the test (blue diamonds on Fig. 78), it is found that the depletion voltage rises with a slope of 0.17 V/day; The test had to be interrupted because of probe station availability and the structure has been biased at room temperature for one day, enhancing reverse annealing due to lack of cooling and high leakage current. Afterwards, the red triangles on Fig. 78 show the follow-up of the test: the structure has been kept biased at low temperature again. the depletion voltage shows a step due to the annealing between the two parts of the test, but went increasing again afterwards.

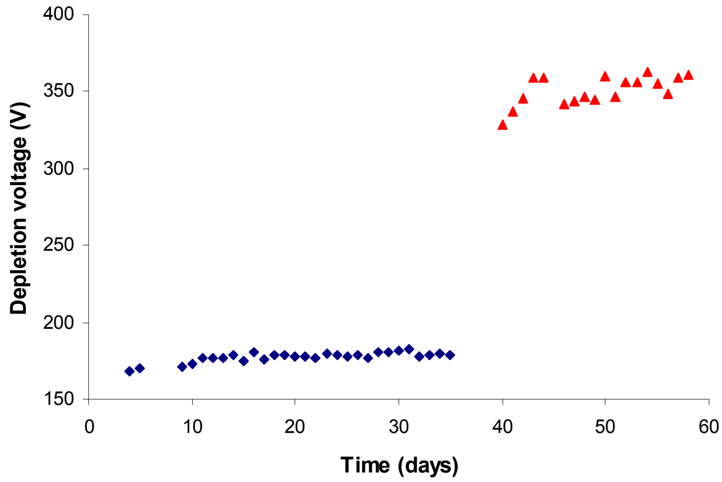

Fig. 78 : Evolution of the depletion voltage of an irradiated thin HPK structure kept biased at 400 V at –10 °C.

Looking at the first part of the test, a difference of 12 V between the initial depletion voltage and the final one is observed. This difference is relatively small but the evolution of the depletion voltages can be observed on the superposition of the kinks observed on the CV curves (Fig. 79).

In [35], the impact of this effect for the Atlas tracker, after 10 years at LHC, is estimated to be between 40 and 70 V, with an "activation rise time" quoted to be about 100 days at –7 °C. Our depletion voltage increase is compatible with such an increase rate as we obtain a 12 V rise in about one third of the time. Indeed, one would obtain an effect in the lower end of the range quoted in [35], due to a slightly lower operating temperature.

It is however regrettable that this test could not have been pursued for a longer period. It would for sure be interesting to perform a longer test over at least 4 months, to be extended as long as the depletion voltage rises. This test could bring a new view on the reproducibility of this effect, its saturation value and would eventually allow to give an estimation on its possible impact on the tracker.

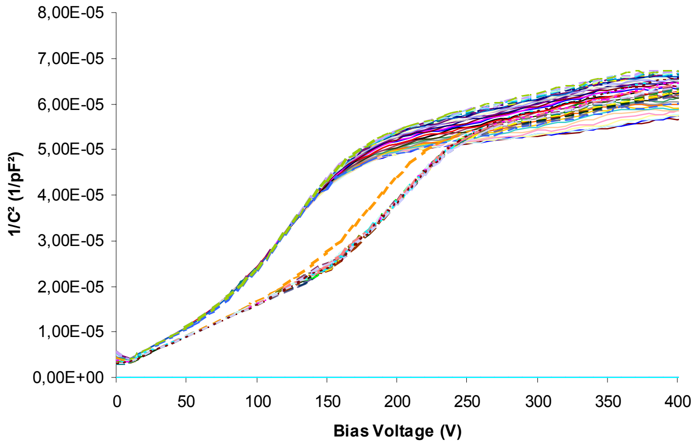

Fig. 79 : CV curves measured during the long term test.

Polysilicon resistances variation under irradiation

As already pointed out above, the polysilicon resistances do not seem to be heavily affected by neutron irradiation. This is confirmed to a larger extent on Fig. 80, where the most affected structures show a decrease of 3% only after a dose equivalent to 15 years at LHC.

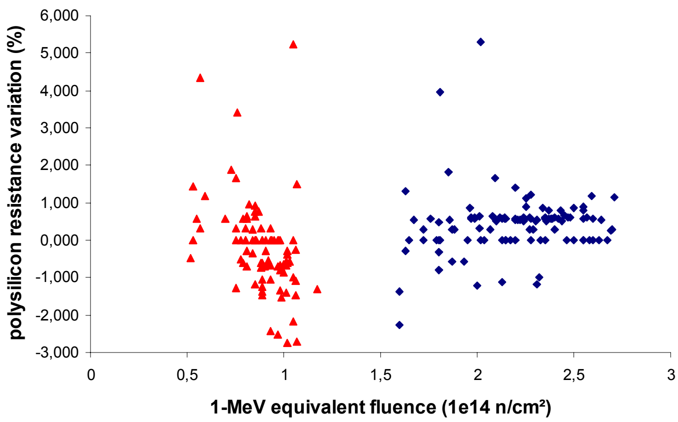

Fig. 80 : R_{poly} variation after irradiation (red triangles for thick structures, blue diamonds for thin ones).

However, it seems that the thick structures may show a decrease of the resistance. This should be further studied at higher doses as the spread of the variation distributions (Fig. 81) does not allow to firmly conclude anything about this so far.

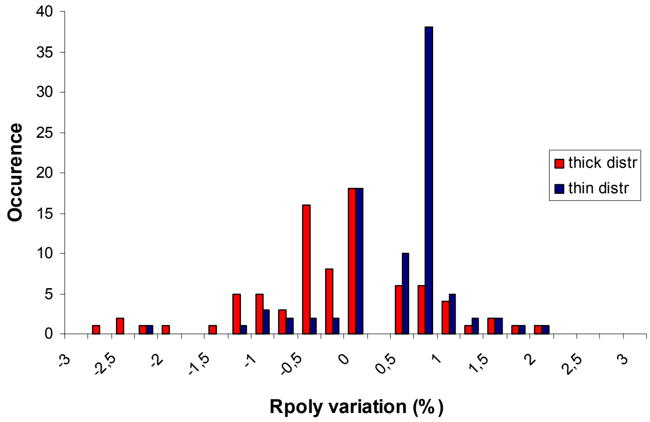

Fig. 81 : Distributions of the polysilicon variations after irradiation for thick and thin structures.

The average variations extracted from these distributions are the following: –0.185 % (3.2 kΩ) for thick structures and 0.64 % (11.1 kΩ) for thin ones with standard deviations of respectively 1.234 % and 1.96 %. These standard deviations are hence compatible with the absence of variation under neutron irradiation, and make our data sample irrelevant to deduce any further trend. Once again this stresses the complementarity of the neutron and proton irradiations performed in the CMS-IQC framework as our result differs from those obtained under proton irradiation where an increase of the bias resistance values is observed (about 350 kΩ and 150 kΩ for thin and thick structures respectively).

Coupling capacitance evolution under irradiation

Fig. 82 shows the evolution of the coupling capacitance as a function of the fluence, as Fig. 80 did it for polysilicon resistances.

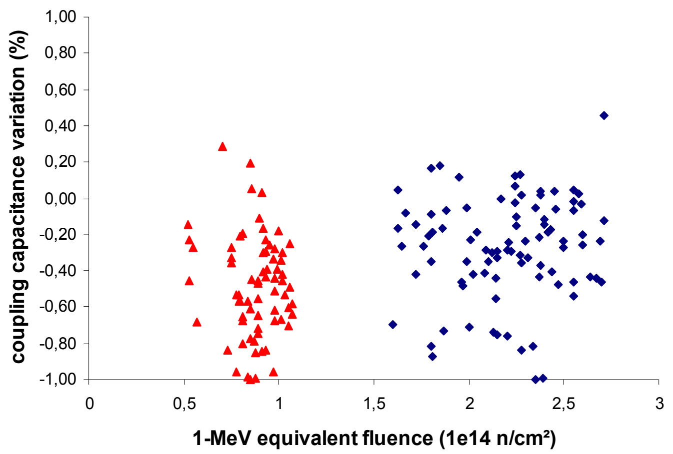

Fig. 82 : coupling capacitance variation expressed as percentage of the initial value for thick (red) and thin structures (blue)

Again, as mentioned when considering the impact of biasing, but this time on a larger sample size, a clear relation between fluence and coupling capacitance variation cannot be deduced although it seems that these capacitances slightly diminish when submitted to a radiation flux (Fig. 83).

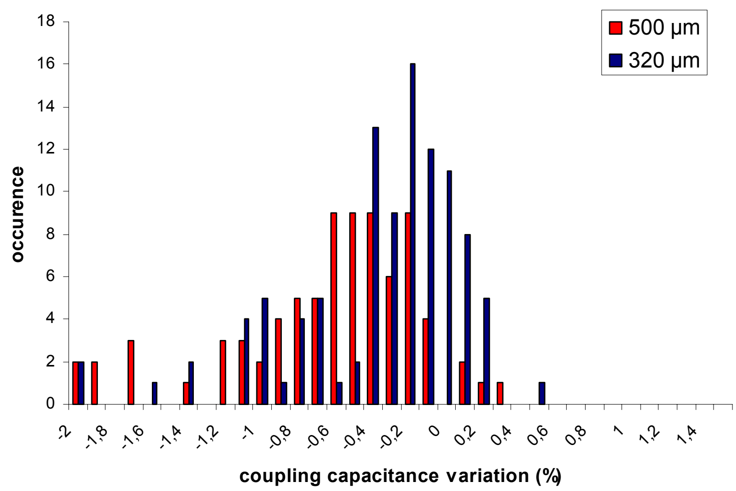

Fig. 83 : coupling capacitance variation distributions.

Indeed, the average variations are of –0.64 % for all data sets (thick, thin or global) and again the spreads are relatively high with standard deviations of 1.68 % for thin structures and 0.96 % for thick ones (the global standard deviation being of 1.45 % considering all structures together). This corresponds to a decrease of 0.07 pF to be compared to a typical decrease of about 1 pF observed on CMS structures under proton irradiation.

Interstrip resistances

Part of the ST production had a low R_{int} problem, but these structures where not irradiated as they did not pass the PQC and QTC steps of the CMS QA procedure. It is then no big surprise that it is found here that almost all tested structures and sensors were fine regarding the 20 MΩ minimal interstrip resistance criteria, apart a few ones which showed an evident other big failure.

As the interstrip resistance value is highly bias-dependent, a detailed analysis requires the individual inspection of the R_{int} versus bias ramp measurement. These ramps, are shown on the following figures, where the bias voltage is normalized to the depletion voltage to give a better idea of the bias status of each structure.

It can be noticed that the curves for the thick structures are similar to each other unlike those of the thin structures, which present more often an earlier increase. This is anyway not a source of concern since it means that the strips of thin structures have a better insulation between them, which is good regarding the noise performance of the sensors.

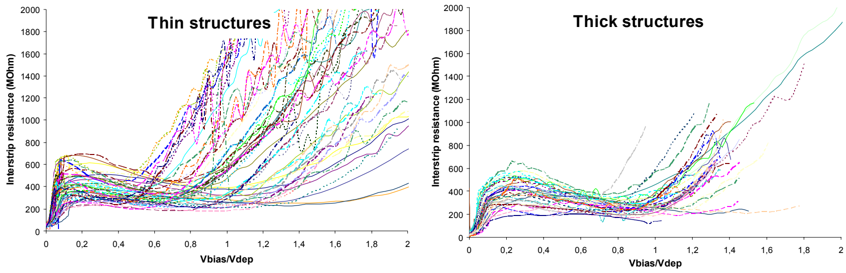

Fig. 84a, b : post-irradiation interstrip resistance as a function of the bias status for thin and thick test structures.

Fig. 85 shows the distribution of the value of the interstrip resistances at the local minima of the above curves, as a function of the fluence. The idea of the analysis is the same as before, and again there is no clear correlation between R_{int} and fluence for the fluences concerned here.

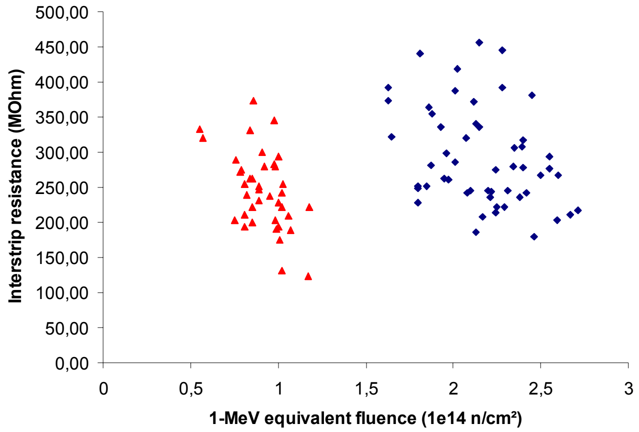

Fig. 85 : value at local minima of the curve.

At same bias status, the difference between thick and thin structures is not evident: respectively 245.6 ± 55 MΩ and 291.8 ± 70.3 MΩ. But it has been shown before that the thin structures generally have lower depletion voltages than thick ones, at a fluence of 10 years operation at LHC. Therefore, at the same bias voltage (400 V), thin structures show an average interstrip resistance of 1560 MΩ whereas thick ones present an average of 620 MΩ, again pointing in the direction of a better strip insulation.

Interstrip capacitance behaviour

In late 2003, a first summary of the results obtained under neutron irradiation had shown that thick structures present a bigger increase of the interstrip capacitance after irradiation. This effect remained constant thereafter as indeed, post-irradiation measurements at 400 V bias indicate that thick structures present an average increase of 0.55 pF whereas thin ones 0.13 pF only.

This is pictured on Fig. 86 for the data collected in 2003 and 2004. On this figure, the increase is expressed as a percentage of the initial interstrip capacitance, around 0.67 pF for all baby detectors.

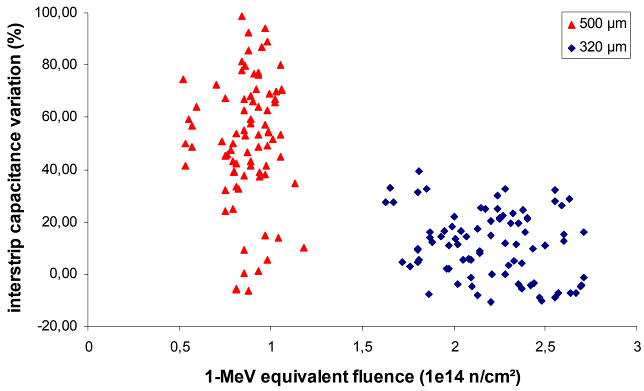

Fig. 86 : interstrip capacitance variation distribution as a function of the fluence.

The effect is further illustrated on the two graphs below. On these graphs, the curves coming from the bottom are the pre-irradiation ramps of the interstrip capacitances as a function of the bias voltage. Curves coming from above show the post-irradiation data. It is clear again that thick structures (on the right) present a higher increase. Furthermore, the end of the ramps are quite flat, suggesting that the saturation value of the interstrip capacitance is reached.

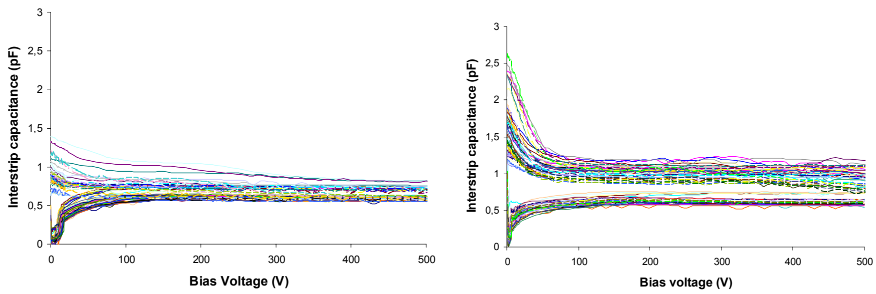

Fig. 87a, b : Interstrip capacitance as a function of the bias voltage for thin (left) and thick (right) structures.

However, as the value of the interstrip capacitance boasts a high dependence on the depletion status of the detector, it has then been decided to perform a few measurements up to very high voltages, in case of an hypothetic further decrease and despite the risk to generate an electrical breakdown on the device. A dedicated irradiation has been performed and the results were cross-checked in Louvain, Karlsruhe and Strasbourg.

The results and measurements before and after this special irradiation where all consistent among the different measurement setups. The above-mentioned effect has been observed on W6 (thick) structures produced both by HPK and STM, proving that it is vendor-independent. Surprisingly, a further decrease of the interstrip capacitance has been observed well above the depletion voltage (Fig. 88).

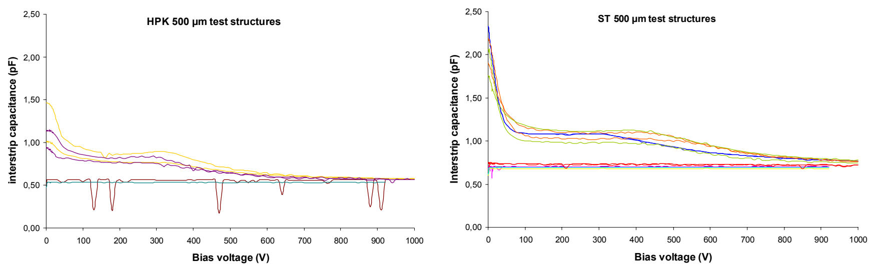

Fig. 88a, b : Interstrip capacitance measurements as a function of bias voltage for HPK (left) and ST (right) thick structures, up to 1000 V.

Strips scans also confirmed that the effect is uniform across a structure. It has therefore been concluded that this variation was linked to the geometry of the sensor, and especially its thickness.

No further investigations on this topic has been carried out. The qualification procedure remained unchanged, but it had been decided within the CMS sensor group to perform additional measurements on the thick structures showing an unusually high C_{int} at 400 V bias. A very interesting study would be to measure the impact of the increase of the interstrip capacitance to the crosstalk between adjacent strips of a complete module.